Journal of Applied Electrochemistry
https://doi.org/10.1007/s10800-025-02352-8

RESEARCH ARTICLE

Exploring linoleic acid as a novel co-adsorbent to enhance dye-sensitized solar cell efficiency through surface engineering of TiO_2 at the photoanode /electrolyte interface

M. A. K. L. Dissanayake[1,2] · P. U. Sandunika[1,2] · G. K. R. Senadeera[1,3] · J. M. K. W. Kumari[1] · M. S. H. Hettiarachchi[1,2] · J. L. Subasinghe[1] · A. K. Karunaratne[1,2] · W. I. Sandamali[1,3]

Received: 15 April 2025 / Accepted: 9 August 2025

Abstract The global energy crisis is driving the search for sustainable energy resources, with solar energy emerging as a leading candidate. While dye sensitized solar cells offer potential as the third-generation solar cells, recombination losses at the photoanode/electrolyte interface limit their performance. This study introduced linoleic acid as a novel co-adsorbent to suppress recombination without slowing down charge injection from dye to TiO_2. Linoleic acid also reduces the formation of dye-I_2 complexes by binding iodine to its double bonds. A dye sensitized solar cell with a TiO_2/Dye/Linoleic acid (0.95 mM) photoanode showed an efficiency of 8.31% under 100 mW cm^{-2} (AM 1.5) illumination, a 25% enhancement compared to the unmodified TiO_2/Dye cell (6.61%). This improvement is attributed to a 38% increase in the short-circuit current density and a red shift in optical absorption due to linoleic acid adsorption. UV–Visible Diffuse Reflectance Spectroscopy revealed new energy surface states introduced by linoleic acid, enhancing electron transport. Electrochemical Impedance Spectra, Cyclic Voltammetry, and Mott–Schottky analysis confirmed reduced recombination, while enhanced incident photon to current conversion efficiency spectra validated the improved photovoltaic performance. It can be concluded that linoleic acid binds to TiO_2 via a bridging bidentate mode, mitigating recombination and boosting dye sensitized solar cells efficiency. These findings highlight linoleic acid's potential to address key challenges in dye sensitized solar cells development.

✉ M. A. K. L. Dissanayake
lakshman.di@nifs.ac.lk; makldis@yahoo.com

P. U. Sandunika
sandunika.pa@nifs.ac.lk

G. K. R. Senadeera
gkrsena@yahoo.com

J. M. K. W. Kumari
kalpani.ku@nifs.ac.lk

M. S. H. Hettiarachchi
sanuri.he@nifs.ac.lk

J. L. Subasinghe
janyalumbini0@gmail.com

A. K. Karunaratne
kaushalyawin93@gmail.com

W. I. Sandamali
ishara9388@gmail.com

[1] National Institute of Fundamental Studies, Hantana Road, Kandy, Sri Lanka

[2] Postgraduate Institute of Science, University of Peradeniya, Peradeniya, Sri Lanka

[3] Department of Physics, The Open University of Sri Lanka, Nawala, Nugegoda, Sri Lanka

Published online: 05 September 2025

Graphical abstract

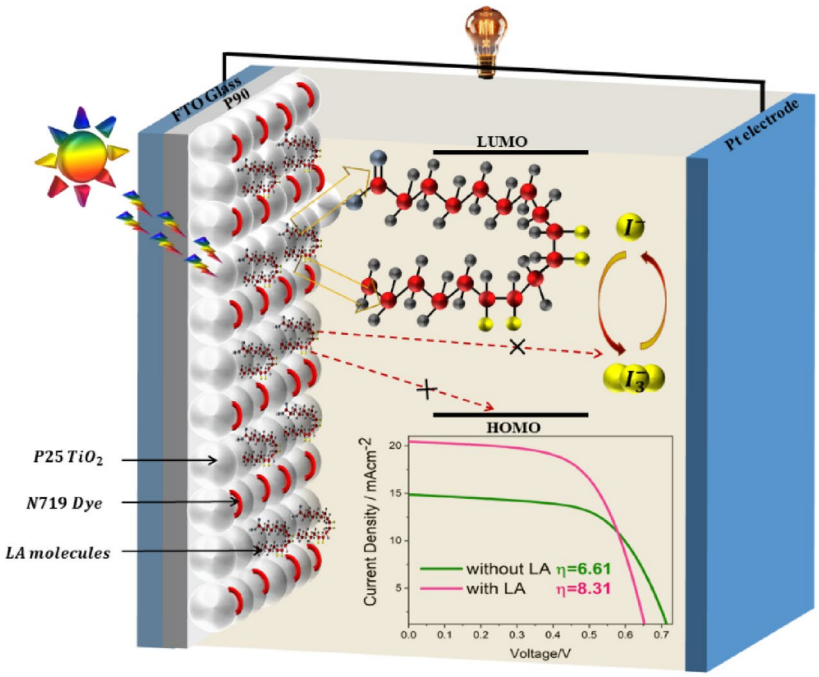

5

Keywords Dye sensitized solar cells · Co-adsorbent · Linoleic acid · Surface modification of TiO_2 photoanode · Reduced recombination

1 Introduction

In recent decades, Earth has been facing an energy crisis primarily due to population growth and the depletion of finite fossil fuel resources. Additionally, the combustion of fossil fuels releases substantial amounts of greenhouse gases and pollutants into the earth, exacerbating climate change, air pollution, and widespread environmental degradation. Consequently, alternative energy sources that are Renewable, eco-friendly, cost-effective, abundant, and sustainable have garnered considerable attention in the recent past. By 2050, demand for fossil fuels is expected to decline by approximately 50%, driven by the increasing prominence of renewable energy sources, including wind, geothermal, and solar, in the global energy portfolio. The Sun, as the most consistent and abundant source of renewable energy, has the potential to provide enough energy in one hour of sunlight to meet the global energy demand for an entire year [1, 2]. Despite the sustainability of solar energy, traditional silicon-based solar cells, which convert the solar energy into electricity, remain expensive and have limited applications. On the other hand, Dye-sensitized solar cells (DSSCs), representing the third generation of solar cells, offer a cost-effective, easily manufacturable, and versatile alternative to conventional solar cells [3]. Since their groundbreaking development by O'Regan and Grätzel in 1991, DSSCs have attracted significant interest, with ongoing research efforts focused on enhancing their efficiency [4–7]. Generally, a DSSC consists of a dye-sensitized nanocrystalline TiO_2 film on a transparent conducting oxide (TCO) glass substrate (photoanode), a platinum counter electrode, and an iodide-triiodide liquid electrolyte. The photoelectrode, sensitized by a Ruthenium bipyridine complex, is separated from the counter electrode by the iodide-triiodide liquid (gel or solid) electrolyte [5, 8, 9]. A DSSC can be a better competitive alternative to other solar cells by further reducing material costs and production methods, while improving device stability and efficiency. Models have been employed to quantitatively identify promising electrolytes (liquid, gel, and solid), dyes, and semiconductors to achieve these goals

[10]. Various factors influence the photovoltaic performance of a DSSC, including electron collection at the photoanode, the efficiency of the photoanode in harvesting light, and the scattering of electrons within the photoanode [11–13].

Many studies have been conducted on the surface modification of the photoanode. These include the modification of the fluorine-doped tin oxide (FTO)/nanocrystalline semiconductor (nc-SC) interface by utilizing a compact layer of semiconductor material that blocks exposed sites of FTO to the electrolyte [14], the modification of the nc-SC/dye interface through acid treatment, which results in enhanced dye loading because of a positively charged surface, or the application of an insulating/semiconducting blocking layer on the nc-SC surface [15], the modification of the nc-SC/dye interface through the use of co-adsorbents, which aids in decreasing dye aggregation and recombination [16], and the modification of the dye/electrolyte interface through the use of additives that provide surface passivation and positive movement of the nc-SC Fermi level [17]. In related endeavors, Das et al. reported the incorporation of a TiO_2 passivation layer between the mesoporous TiO_2 nanoparticle layer and the conducting glass surface using a simple dip coating method [18]. Fei et al. reported a facile surface modification technique for ZnO aggregates that led to a notable increase in efficiency. This process involves the introduction of a thin layer of TiO_2 nanoparticles on the surface of ZnO aggregates to reduce the charge recombination and increase the charge collection. As a result, the ZnO aggregate-based DSSCs showed a 30.3% efficiency enhancement [19]. Nath et al. reported that the use of phenylalkonic acid as a co-adsorbent resulted in enhanced efficiency, which correlated with an increase in the chain length of the hydrophobic alkyl groups [20]. Furthermore, Wang et al. reported similar work for decylphosphonic acid [21]. Anantharaj et al. modified the dye-adsorbed TiO_2/electrolyte interface by co-adsorption of oleic acid (OA) over the TiO_2 surface, and the modified cell exhibited a higher efficiency (η) of 12.9% [22]. Mazloum et al. investigated the effects of oleic acid as a dual-function co-adsorbent on recombination and reduced the surface concentration of the dye-iodine complex by saturating the bond of OA with iodine present in the electrolyte [9]. Magne et al. optimized dye loading and reduced recombination in DSSCs by testing various fatty acids as co-adsorbents with the sensitizer. Butyric acid and octanoic acid, with compatible alkyl chain lengths and efficient regeneration of oxidized dye by iodide, achieved the highest efficiencies [8]. Saxena et al. presented a comprehensive study on the treatment of TiO_2 surfaces by different carboxylic acids, including formic acid (FA), oxalic acid (OA), and citric acid (CA) [7]. Xin Li et al. utilized pivalic acid as a novel co-adsorbent to modify the interface between the photo anode and electrolyte, which can be used to enhance the performance of the DSSCs by 8% [23]. Şahingöz, R. et al. performed a high efficiency with showing 43.45% increase by using 1-naphthalenetic acid (NAA) as a co-adsorber to the N719 dye [24]. Rodrigues et al. presented the use of polymeric co-adsorbents PVBA and P4VP as alternatives to CDCA, achieving photovoltaic performance of up to 9% [25].

Various approaches have been attempted to modify the photoanodes of DSSCs using carboxylic acids, as mentioned in previous paragraphs. These acids can be categorized into two types: amino acids and fatty acids. To the best of our knowledge, while carboxylic acids with different chain lengths have been investigated, the effect of the number of double bonds in carboxylic acids has not yet been explored. For this purpose, building upon previous research work, we propose a novel material, Linoleic acid (LA), which is an octadecadienoic acid in which the two double bonds have Z (cis) stereochemistry.

Figure 1 shows the chemical structure of the LA. As shown in Fig. 1, it is an omega-6 fatty acid with a long chain and double bonds at positions 9 and 12, which are expected to mitigate recombination at the interface between the photoanode and electrolyte caused by iodine binding to those two double bonds of LA, as well as to enhance the charge injection rate from the dye molecule to the semiconductor.

LA molecules selectively adhere to the exposed surface of TiO_2, not occupied by dye molecules. Consequently, the entire available TiO_2 surface becomes covered by dye and LA molecules. These LA molecules are anticipated to hinder recombination processes occurring at the TiO_2/electrolyte interface without affecting the charge injection from the photoexcited dye molecules to TiO_2. Moreover, we have observed that the interaction between iodine and LA through its double bonds affects the enhancement efficiency. In the present work, this approach has resulted in enhanced power conversion efficiency (PCE) of 8.3%. It should be mentioned here that the impact of varying numbers of double bonds in carboxylic acids remains largely unexplored, which is needed to address the research gap. The present work can be the first step towards such a comprehensive long-term study.

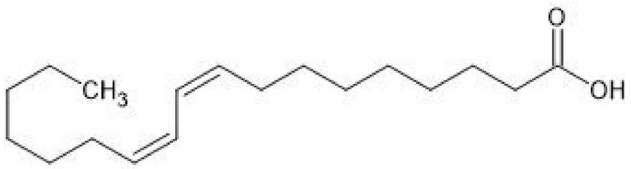

Fig. 1 Chemical structure of LA

2 Experimental

2.1 Materials

All chemicals used in this study were of analytical reagent grade. Titanium dioxide powder TiO_2 P25 was purchased from Degussa AG, and aeroxide TiO_2 P90 powder, which has an average particle size of about 10–14 nm, was purchased from Evonik. LA was purchased from Sigma Aldrich. Fluorine-doped tin oxide (FTO) conducting glass (Solaronix sheet glass, sheet resistance 8 Ω sq^{-1}) and Ruthenium dye N719 [RuL2(NCS)2:2TBA (L=2,2′-bipyridyl-4,4′-dicarboxylic acid)] were purchased from Solaronix. Triton X-100 nonionic surfactant (laboratory grade, cat. no. 9002-93-1), poly(ethylene glycol) (PEG, 99.8%, Mw=2000 g mol^{-1}), and nitric acid (HNO_3, 69%) were purchased from Merck. Ethanol absolute (anhydrous>99.8%) was purchased from VWR Chemicals. Ethylene carbonate (EC 98%), tetrapropylammonium iodide (Pr_4NI, 98%), iodine (I_2>99%), and acetonitrile (anhydrous) were purchased from Merck. All of the materials used in this study were used without further purification.

2.2 Photoanode preparation

The detailed method of fabricating the series of photoanodes is as follows: The FTO glasses were cut into 1×2 cm^2 rectangular pieces and cleaned by using a mixture of conc. HNO_3 and distilled water in an ultrasonic bath. They were subsequently cleaned by boiling with isopropyl alcohol. To prepare the compact layer, 0.25 g of TiO_2 P90 powder with 1 ml of 0.1 M HNO_3 was finely ground for 15 min, and the paste was spin-coated at 3000 r.p.m. on the conductive side of the cleaned FTO glass and sintered at 450 °C for 45 min. To prepare the TiO_2 P25 paste, 0.25 g of TiO_2 powder and 1 ml of 0.1 M HNO_3 were ground using a mortar and pestle. Subsequently, 0.02 g of Triton X-100 and 0.05 g of polyethylene glycol 2000 (PEG) were applied as a binder, and the mixture was finely ground until it became a creamy paste. The TiO_2 P25 paste was placed on the FTO/TiO_2 P90 electrode by the doctor-blade technique to obtain a smooth and flat surface using adhesive tape, and the electrode was sintered at 450 °C for 45 min. The N719 dye was used in this study due to its capacity to absorb visible light, high molecular ability, and prospective photovoltaic performance.

The prepared TiO_2 electrodes were dipped into the solution of 0.03 mM Ruthenium N719 dye dissolved in ethanol for 24 h, kept at room temperature in the dark to allow the dye to attach to the TiO_2 surface. The dye-coated photoanodes were washed thoroughly with absolute ethanol and dried to remove excess dye molecules. For the preparation of the LA-anchored TiO_2 photoanode, the dye-coated photoanode films were dipped in a mixture of absolute ethanol and LA for three hours. They were then washed thoroughly with absolute ethanol and dried prior to fabricating the solar cells.

To achieve the best DSSC performance with the highest efficiency, the fabricated photoanodes were subjected to several optimizations, such as LA concentration and photoanode dipping time in LA. To optimize the LA concentration, different solutions were prepared by dissolving LA in ethanol at concentrations of 0.75 mM, 0.85 mM, 0.95 mM, 1.05 mM, and 1.15 mM. Among these, the best LA concentration was found to be 0.95 mM, yielding the highest DSSC efficiency. For further optimization, dye-attached TiO_2 photoanodes were dipped for varying times in 0.95 mM LA solution, and their DSSC performance was evaluated.

2.3 Electrolyte preparation

For the preparation of the Liquid electrolyte containing the redox couple, 0.738 g of tetra-propyl ammonium iodide (Pr_4NI) and 0.060 g of iodine (I_2) were added to a precleaned bottle containing 3.6 ml of melted ethylene carbonate (EC) and 1.0 ml of acetonitrile. This solution was stirred at room temperature until all solid compositions dissolved and kept under constant stirring overnight, and used to fabricate DSSCs.

2.4 DSSC fabrication

To fabricate the solar cell, the liquid electrolyte was sandwiched in between the pristine TiO_2/dye or LA-anchored TiO_2/dye photoanode and the platinum counter electrode. For this, the photoanode and the counter electrode were directly stacked and held together by gently pressing with two alligator clips to ensure proper contact. The electrolyte was introduced by carefully injecting it into the cell through capillary action, which allowed the electrolyte to spread evenly between the two electrodes. The active cell area of the fabricated device was 0.16 cm^2. To ensure the repeatability in the performance of the device, a minimum of five solar cells of each type were made, and the performance of each was evaluated by current-voltage measurements.

2.5 Characterization of materials and devices

Optical absorption measurements of the TiO_2 photoanodes were performed by using the Shimadzu 2450 UV–VIS spectrophotometer. Attenuated total reflection infrared (ATR-IR) spectra were obtained using a Nicolet iS50 (Thermo Scientific) FTIR spectrometer. Current-voltage and impedance measurements of fabricated DSSCs were carried out under simulated sunlight of 100 mW cm^{-2} with the AM 1.5 filter

by using the Autolab potentiostat/galvanostat PGSTAT128 N. Electrochemical impedance spectra (EIS) of DSSCs were obtained by using the frequency response analyzer (Metrohm) in the frequency range between 0.01 Hz and 1 MHz under the same simulated light intensity at room temperature.

Cyclic voltammetry tests were conducted for photoanodes, employing a three-electrode setup consisting of a Pt wire as the counter electrode, an Ag/AgCl electrode as the reference electrode, and either TiO_2/Dye photoanode or a LA-anchored TiO_2/Dye photoanode as the working electrode. A supporting electrolyte comprising an acetonitrile solution with 10 mM LiI, 1.0 mM I_2, and 0.1 M $LiClO_4$ was utilized, employing a scan rate of 0.05 V/s. Monochromatic light illumination via the Bentham PVE300 unit, comprising a TMC 300 monochromator-based IPCE system with a 150 W Xenon arc lamp covering the 300–800 nm wavelength range, was used to measure the incident photon to current conversion efficiency (IPCE) of the DSSCs.

3 Results and discussion

3.1 Optical absorption measurement analysis

The essential factor contributing to the photovoltaic performance in DSSCs is the broad light absorption range of the sensitizer, which covers the wavelengths from visible to near-IR regions. Figure 2a compares the optical absorption spectra of dye-adsorbed TiO_2 photoanodes with and without LA modification. A notable observation is the significant red shift in the absorption spectrum following LA modification. This shift may indicate a rearrangement of dye molecules already anchored on the TiO_2 surface during LA adsorption. Dye molecules can aggregate either before being adsorbed onto the photoanode surface during DSSC fabrication or afterward. This aggregation can significantly impair the performance of a DSSC device. Generally, the aggregation between dye molecules can be classified as H-aggregates (face-to-face arrangements) and J-aggregates (edge-to-edge arrangements). J-aggregates formed in an edge-to-edge

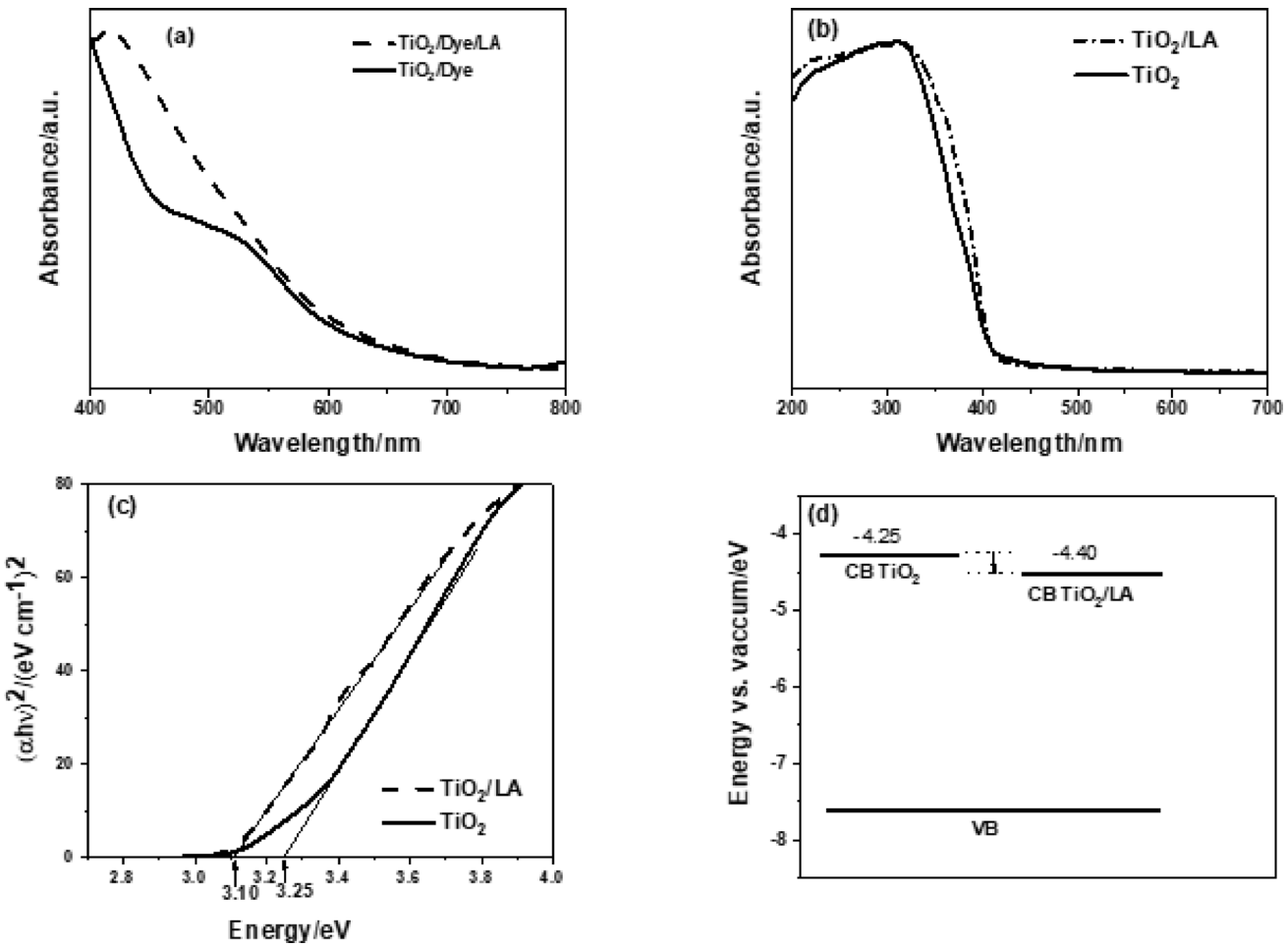

Fig. 2 **a** UV–vis absorption spectra of TiO_2/dye and LA-anchored TiO_2/dye photoanodes. **b** UV–Vis optical absorption spectra derived from diffused reflectance of the pristine TiO_2 powder and LA anchored TiO_2 powder, and **c** Tauc plots applied to absorption spectra shown in (**b**). **d** Energy level diagram for pristine TiO_2 powder and LA anchored TiO_2

alignment when dye molecules aggregate, cause a bathochromatic shift (red shift) in the optical absorption spectra. These aggregations depend on solvent polarity, dye concentration, pH, and temperature [26].

The absorption spectra of the LA-anchored TiO_2/Dye photoanode were slightly broadened due to the existence of J-aggregates [22, 27, 28] and red-shifted, indicating low aggregation on the TiO_2 [29]. The presence of an additive favors the formation of J-aggregates in the dye, leading to a red shift in its optical absorption [26]. Through the treatment with LA, it becomes feasible to remove excessively aggregated dye molecules from the TiO_2 surface as LA can break up these dye aggregates and make them soluble in the solvent. The mechanism behind this involves LA molecules competing with dye molecules for adsorption sites on TiO_2, thereby spacing the dyes apart and disrupting the π–π stacking interactions. This co-adsorption effect leads to a significant reduction in intermolecular interactions, which is crucial for efficient electron injection. Similar mechanisms have been observed in studies involving other co-adsorbents such as deoxycholic acid (DCA), where dye aggregation was suppressed and spectral red-shifting occurred, indicative of weakened π–π interactions [30, 31].

In order to understand the red shift observed in the optical absorption spectrum due to LA adsorption on the TiO_2 surface, the UV–Vis absorption spectra obtained from the diffused reflectance (DR UV–Vis) measurements of both pristine TiO_2 powder and LA-anchored TiO_2 powder samples, as shown in Fig. 2b can be analyzed. As shown in Fig. 2b the absorbance of the LA-anchored TiO_2 powder exhibit a slight increase across the visible spectrum. The increased absorption from the band edge into the visible range indicates the formation of intermediate states. To observe this, DR UV–Vis for LA-anchored TiO_2 powder samples was measured using pristine TiO_2 powder as a reference for their baseline correction. This spectrum is shown in Fig. S1 (Supplementary Information).

This increased absorbance may result in creating intermediate states, as observed in the interfacial modification between the photoanode and electrolyte interface in DSSC using oleic acid by Anantharaj et al. [22]. Similar observations have been made in the study of oleic acid anchored ZA:0.01Eu^{3+} by Miller et al., BPEu-MoNo/ BPEu-Hexa by Sekar et al., and $LaPO_4$:Eu^{+} by Liping et al. [32–34]. In the present study, LA-anchored TiO_2 showed a significant increase in absorbance from 800, peaking around 366 nm (Fig. S1). This indicates the formation of new intermediate states through LA adsorption on TiO_2, which may contribute to electron transport by introducing mid-energy levels [22, 32, 33].

While DSSC photoanodes are generally semi-transparent, the films used in our study may exhibit surface irregularities and scattering due to their nanostructured TiO_2 nature. Therefore, absorbance/transmittance methods may not fully capture the optical behavior of the films. DR UV–Vis spectroscopy effectively collects scattered light from irregular surfaces, ensuring accurate optical characterization. This helps to generate reliable Tauc plots and estimate the optical band gap [35–37].

The energy band gap (E_g) was determined using the equation S1 (supplementary information). Tauc plots applied to the absorption spectra shown in Fig. 2b reveal calculated energy band gaps are 3.25 eV for pristine TiO_2 and 3.1 eV for the LA-anchored TiO_2. The value for pristine TiO_2 is consistent with reported literature values [38–40].

The highest valence band of anatase nanocrystals has been previously evaluated and determined to be − 7.5 eV [41]. It has also been reported that the energy level of the highest valence band of P25 TiO_2 is nearly identical to that of anatase. Therefore, the energy levels of the conduction band and the highest valence band for pristine TiO_2 and LA-anchored TiO_2 photoanodes can be determined, assuming that the energy levels of their highest valence bands are the same at − 7.5 eV [7, 42, 43]. Assuming a valence band position at − 7.5 eV, the conduction band edges of pristine TiO_2 and LA anchored TiO_2 photoanodes are estimated to be 4.25 eV and 4.4 eV, respectively. Based on these results, an energy level diagram, as shown in Fig. 2d, was deduced for pristine TiO_2 and LA-anchored TiO_2 photoanodes. According to Fig. 2, the LA-anchored TiO_2 photoanode shows that the edge of the conduction band shifts away from the vacuum level, resulting in lower values of open circuit voltage (V_{OC}). This will be further analyzed in the cyclic voltammetry section.

These findings are consistent with previous reports in the literature, further supporting the idea that surface modification can significantly affect the properties of TiO_2. A similar trend has also been reported by Anantharaj et al. in his studies for oleic acid modified photoanode [22].

O'regan et al. [44] provided direct evidence of dye-iodine binding to the N719 dye through its thiocyanate (NCS) group. They demonstrated that when iodine binds to the NCS ligands, it decreases the energy of the HOMO, causing a blue shift in HOMO-LUMO transitions such as the visible and UV MLCT (metal-to-ligand charge-transfer) bands. To investigate this phenomenon further, we studied the interaction between iodine molecules with dye and LA. The absorption spectra of TiO_2/Dye film in a mixture of absolute ethanol solution alone or with iodine and LA are depicted in Fig. 3.

In Fig. 3, a 13 nm blue shift in intensity from the MLCT peak at 538 nm to a new peak at about 525 nm is observed. Upon the addition of LA to the solution, a 5 nm red shift in the peak can be noted from 525 nm to 530 nm. The blue shift

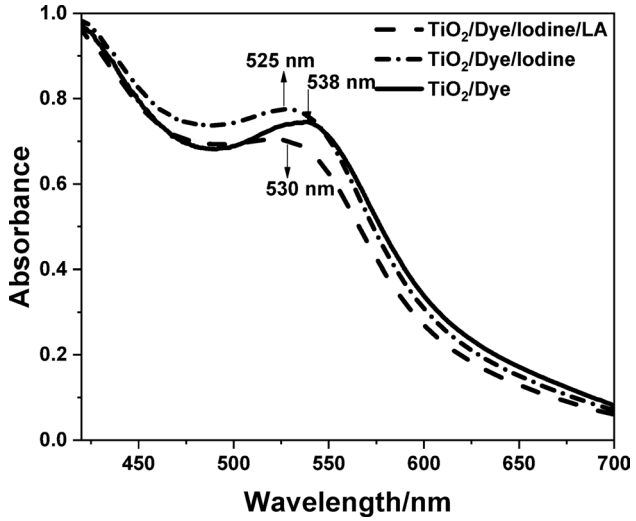

Fig. 3 The absorption spectra of N719 Dye film in mixture of absolute ethanol solution alone or with iodine and LA

Table 1 Shift in the peak wavelength of the TiO_2/dye film in an absolute ethanol solution, either alone or mixed with iodine and LA

Photo anode	Wavelength at peak (nm)
TiO_2/Dye	538
TiO_2/Dye/Iodine	525
TiO_2/Dye/Iodine/LA	530

in the absorbance spectrum may result from a decrease in HOMO energy and/or an increase in LUMO energy, while the red shift in absorbance may result from iodine being bound to the unsaturated double bonds on LA. Based on these results, it can be suggested that the adsorption of LA on the TiO_2 surface, leading to red shifts in the peak, is very likely due to iodine binding to the unsaturated double bonds on LA. Therefore, the interaction between iodine and the double bonds of LA appears to keep the iodine molecules away from the thiocyanate group of the dyes (Table 1).

3.2 FTIR analysis

In order to better understand how LA molecules bind to the TiO_2 surface, FTIR characterization was performed on pristine TiO_2, pure LA, and LA-anchored TiO_2 samples using attenuated total reflectance mode (ATR-FTIR mode) [45]. Results are shown in Fig. 4; Table 2.

A distinctive peak appeared at 1709 cm^{-1} in the pure LA spectrum, attributed to the carbonyl stretching mode of the carboxylic acid group. In the FT-IR spectrum of TiO_2/LA, the absorption Due to the carbonyl stretching mode of LA at 1709 cm^{-1} disappeared and was replaced by a new absorption band at 1640 cm^{-1}. This shift suggests that the LA molecules are chemically bonded to the TiO_2 surface rather than by simple physisorption [22]. The carboxylate peaks appeared near 1640 cm^{-1} and 1548 cm^{-1}, which represent

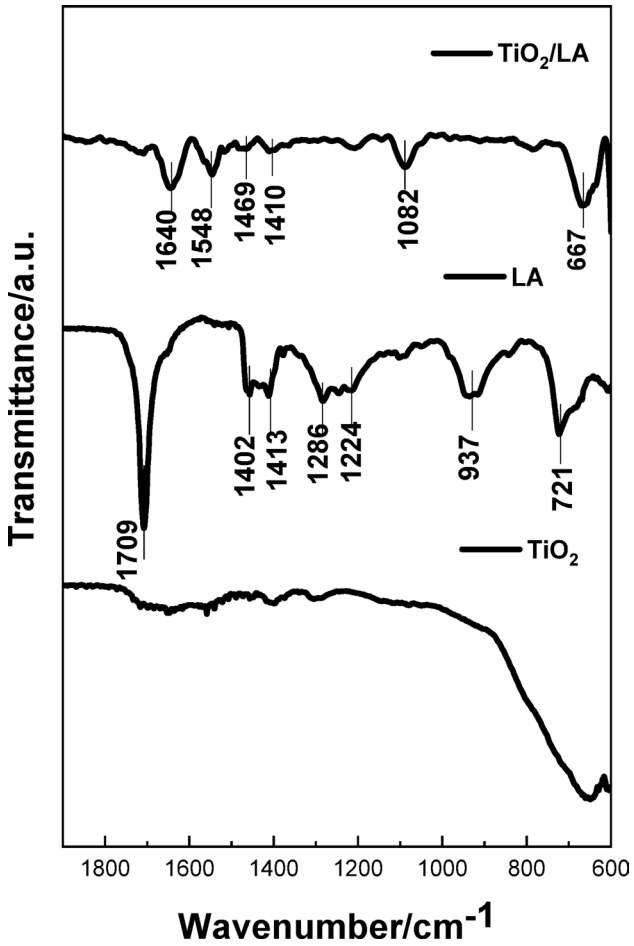

Fig. 4 ATR-FTIR spectra of pure LA, pristine TiO_2 and LA-anchored TiO_2

asymmetric carboxylate stretching (n (COO−)asym) and symmetric carboxylate stretching (n (COO−)sym), respectively. The difference between these two carboxylates stretches gives the value of $\Delta = 92$ cm^{-1}, illustrating that LA molecules are bound to titanium atoms through bidentate chelating modes [35, 46, 53]. The carboxylic acid binding mechanism on metal centers can be inferred from the metal-carboxylate band in the 1300–1700 cm^{-1} range. The carboxylate anion (−COO−) shows asymmetric and symmetric stretching bands due to its coordination with the "Ti" centers. The difference in wavenumbers between the asymmetric and symmetric stretching bands in the metal carboxylate band region can be used to infer the binding nature of the carboxylate anion on the TiO_2 surface, which can be deduced from the difference in the wavenumbers between the asymmetric and symmetric stretching bands [54].

3.3 Photovoltaic performance

The effect of LA on the photovoltaic performance was studied by fabricating DSSCs with TiO_2/Dye photoanodes and

Table 2 Peak assignments and interpretation of the IR spectrum

Wavenumber (cm^{-1})	Peak assignment	Interpretation	References
1709	C=O stretching of carboxylic acid (pure LA)	Indicates free carbonyl groups in LA before binding to TiO_2	[22]
1640	Asymmetric stretching of carboxylate (ν(COO^-) asym)	Suggests chemical bonding of LA to TiO_2 surface, replacing the original carbonyl stretching peak	
1548	Symmetric stretching of carboxylate (ν(COO^-)sym)	Associated with bidentate chelating binding mode of carboxylate anion to Ti centers	[35, 46, 47]
1413	Umbrella stretching mode of $–CH_3$ group	Characteristic of methyl groups in LA	[22]
721	Rocking mode of $–CH_2$ groups	Indicates the presence of methylene groups in LA	
1082	ν(Ti–O–C) bridging vibrations	Represents the interaction between Ti and LA through isopropoxy groups	[48]
667	Ti–O stretching vibration	Represents the Ti–O bond in TiO_2, confirming the presence of titanium oxide in the sample	[49]
1469	$–CH_2$ vibration	Bending vibrations in LA	[50]
1286	C–H bending / C–Hand C–C bending vibrations	Reflects interaction between TiO_2 and organic groups like LA	[50]
1224	C–O vibration	Suggests the binding of organic molecules to TiO_2 or interactions at the TiO_2 surface	[51]
937	Out of plane O–H stretch	Represents the bending vibration of hydroxyl groups	[52]

LA-anchored TiO_2/Dye photoanodes under simulated AM 1.5 solar irradiation with a Light intensity of 100 mW cm^{-2}.

Figure 5a shows the photocurrent density vs. voltage (*J–V*) characteristics of DSSCs with an effective area of 0.16 cm^2. The optimized LA concentration of 0.95 mM was determined through experimentation with DSSCs using TiO_2/Dye photoanodes modified with varying LA concentrations (0.75, 0.85, 0.95, 1.05, and 1.15 mM). As observed in the Fig. 5a, a marked improvement in photocurrent density (J_{SC}) is evident in the device utilizing the LA-anchored TiO_2/Dye photoanode. The photovoltaic parameters obtained from the *J–V* measurements of DSSCs made with TiO_2/Dye photoanode and LA-anchored TiO_2/Dye photoanode are compared in Table 3. The power conversion efficiency of each DSSCs (η) was calculated using Eq. 2 (supplementary information).

The TiO_2/Dye photoanode-based device shows J_{SC} = 14.9 mA cm^{-2}, V_{OC} = 728 mV, *FF* = 60.94% and η = 6.61%, respectively. Following treatment with LA, the optimized TiO_2/Dye/LA photoanode-based DSSC (0.95 mM) shows J_{SC} = 20.5 mA cm^{-2}, V_{OC} = 662 mV, *FF* = 61.18% and η = 8.31%, respectively. Notably, the modified TiO_2/Dye/LA device with 0.95 mM LA exhibits an approximately 38% increase in J_{SC} values, leading to a 25% overall efficiency improvement. The DSSC with the lowest LA concentration (0.75 mM) reached a PCE of 7.31%. Increasing the LA concentration to 0.85 mM resulted in an improved PCE of 7.41%. However, further increases to 1.05 mM and 1.15 mM led to decreased PCEs of 7.79% and 7.55%, respectively. Therefore, the optimal LA concentration in this study was determined to be 0.95 mM.

The higher J_{SC} value is attributed to several factors, such as reduced recombination of injected electrons with the oxidized electrolyte, improved optical absorption, altered electronic structure, efficient charge injection from dye to TiO_2, and enhanced charge transport kinetics, all caused by the adsorption of LA molecules on the TiO_2 surface. Anantharaj et al. reported that the decrease in V_{OC} with increasing LA concentration could be due to the downward shift in the quasi-Fermi energy (E_f) level of TiO_2 [22]. Liu et al. have found that the reduction of V_{OC} was dependent on the density of activated carboxylic acid side groups in their work [55]. In this study, the reduction in V_{OC} may also depend on the density of activated carboxylic acid side groups in LA and the downward shift in the quasi-Fermi energy (E_f) level of TiO_2.

To optimize the photoanode dipping time in LA solution, TiO_2/Dye/LA (0.95 mM) photoanode based devices were measured by varying different times (1, 2, 3, 4, 5 h). The *J–V* curves and their characteristics of these DSSCs are presented in Fig. 5b, and Table 4.

The drop in efficiency after more than 3 h of dipping the photo anodes into LA could possibly be due to over-adsorption of the acid onto the TiO_2 surface, which blocks further dye loading and adversely affects the redox reaction of iodine.

The *J–V* curves of the optimized TiO_2/Dye/LA and TiO_2/Dye photoanodes-based DSSCs are presented in Fig. 5c; Table 5. In Table 5, we have also compared our data with oleic acid modified TiO_2/Dye/OA photoanode reported by Anantharaj et al. [22].

As summarized in Table 5, a significant increase in J_{SC} of the TiO_2/Dye/LA photoanode based DSSC (20.50 ± 0.83) can be observed when compared with the TiO_2/Dye photoanode based device (14.90 ± 0.12). This increase can be

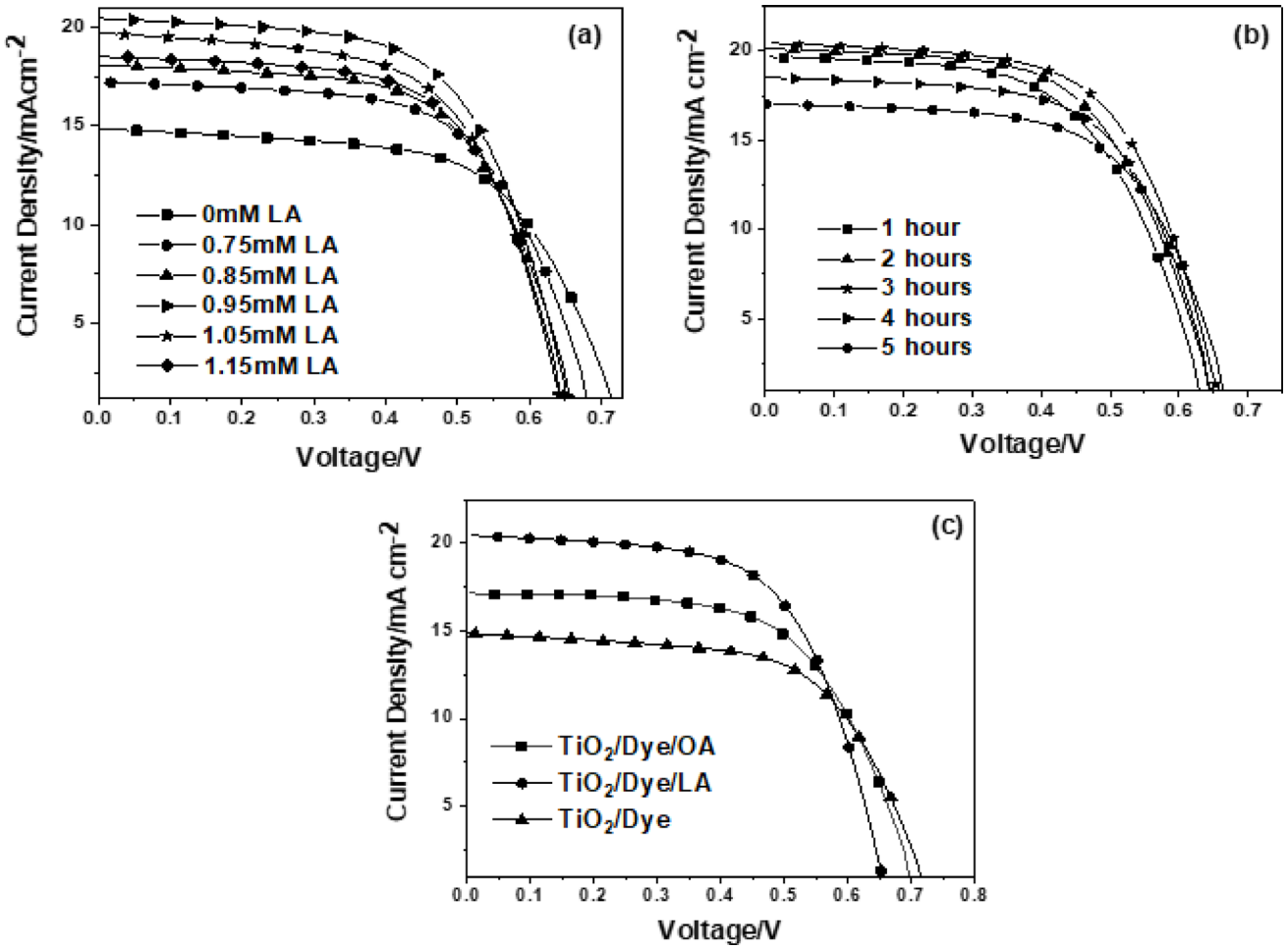

Fig. 5 The current density–voltage curves of the DSSCs with **a** TiO_2/Dye photoanode and LA anchored TiO_2/Dye photoanode, **b** varying LA dipping time, **c** TiO_2/Dye, TiO_2/Dye/LA, and TiO_2/Dye/OA photoanodes under AM 1.5 simulated sunlight illumination

Table 3 Current density–voltage characteristics of DSSCs with TiO_2/Dye photoanode and LA anchored TiO_2/Dye photoanode

Photoanode	V_{OC} (mV)	J_{SC} (mA cm^{-2})	FF (%)	η (%)
TiO_2/Dye	728.00±6.11	14.90±0.12	60.94±1.18	6.61±0.03
TiO_2/Dye/LA (0.75 Mm)	680.14±30.19	17.40±0.53	61.55±0.50	7.31±0.11
TiO_2/Dye/LA (0.85 mM)	669.37±14.59	18.07±0.73	61.25±0.43	7.40±0.22
TiO_2/Dye/LA (0.95 mM)	662.00±31.53	20.50±0.83	61.18±0.44	8.31±0.29
TiO_2/Dye/LA (1.05 mM)	654.38±11.69	19.65±0.95	60.85±0.51	7.79±0.17
TiO_2/Dye/LA (1.15 mM)	648.88±11.19	19.02±0.89	60.93±1.06	7.55±0.30

Table 4 Current density–voltage characteristics of DSSCs with TiO_2/Dye photoanode or LA anchored TiO_2/Dye photoanode, varying dipping time

Time (h)	V_{OC} (mV)	J_{SC} (mA cm^{-2})	FF (%)	η (%)
1	629.84±24.80	19.32±0.94	58.11±1.59	7.30±0.16
2	653.48±11.17	19.86±0.48	59.65±1.16	7.81±0.07
3	662.00±31.53	20.50±0.83	61.18±0.44	8.31±0.29
4	651.75±11.50	18.66±1.14	61.25±1.30	7.45±0.31
5	662.92±15.87	17.23±0.38	61.74±0.81	7.09±0.05

Table 5 The current density–voltage characteristics of the DSSCs with TiO_2/Dye, TiO_2/Dye/LA, and TiO_2/Dye/OA photoanode [22]

Photoanode	V_{OC} (mV)	J_{SC} (mA cm^{-2})	FF (%)	η (%)
TiO_2/Dye	728.00±6.11	14.90±0.12	60.94±1.18	6.61±0.03
TiO_2/Dye/OA (0.95 mM) [19]	702.00±12.54	17.16±0.84	60.78±0.42	7.33±0.18
TiO_2/Dye/LA (0.95 mM)	662.00±31.53	20.50±0.83	61.18±0.44	8.31±0.29

due to the higher interaction between the two C=C double bonds of LA and iodine compared to the interaction between the single C=C bond of oleic acid and iodine. The observed increase in J_{SC} is also related to the enhancement in charge transfer efficiency at the TiO_2/Dye interface due to LA modification. LA molecules might promote the electron injection efficiency from the dye to the TiO_2, as they can improve the electron mobility by passivating surface defects and promoting better electron extraction. The increased J_{SC} indicated that more electrons/sec are injected into the TiO_2 conduction band upon light absorption. Additionally, LA molecules may help in forming a more stable and efficient dye-sensitized layer, leading to improved charge collection at the photoanode [5, 22]. Mazloum et al. [9] have suggested evidence for an interaction between iodine and oleic acid via the double bond of oleic acid. They found that the adsorption of oleic acid on the TiO_2 surface decreases recombination due to iodine binding to the double bond of oleic acid, thereby enhancing the performance of DSSCs. Barea et al. have proven that the increase in π-conjugation in the dye molecule leads to a broader spectral response, increased injection current, and lower open circuit voltage [56].

However, the V_{OC} showed a decreasing trend (TiO_2/Dye: 728.00 ± 6.11mV; TiO_2/Dye/OA: 702.00 ± 12.54; TiO_2/Dye/LA: 662.00 ± 31.53), which can be attributed to the modification of the TiO_2 surface by the LA molecules. The LA molecules likely affect the electron density at the TiO_2/Dye interface, which can change the Fermi level of the TiO_2 and the regeneration process. The interaction between LA and TiO_2 might cause a shift in the energy levels, which can lower the potential difference between the TiO_2 conduction band and the redox electrolyte potential. As a result, the V_{OC} is reduced. Additionally, the adsorption of LA may also inhibit the recombination of photo-generated electrons with holes in the electrolyte, which could further lower V_{OC}.

Table 6 presents a comparative analysis of various DSSCs utilizing co-adsorbent-modified photoanodes, as reported by different research groups in the literature.

3.4 IPCE analysis

The efficiency of a solar cell in converting incoming photons into photocurrent at various wavelengths is quantified by the incident photon to current conversion efficiency (IPCE), which, in the present study, gives an insight into the increased J_{SC} in the presence of LA. As seen from Fig. 6, devices with LA co-adsorbent exhibit enhanced IPCE performance over the entire wavelength range measured.

According to the results of the IPCE measurements, the maximum quantum efficiency peak height for the DSSC made with LA anchored TiO_2/Dye photoanode is 82% at 535 nm. This is significantly higher compared to the peak height of 60% at 530 nm for the DSSC made with pristine TiO_2/Dye photoanode. This enhancement in the quantum yield can be attributed to reduced dye aggregation facilitated by LA, which minimizes intermolecular energy transfer and enhances electron injection efficiency. Accordingly, it offsets the loss of light harvested due to lower coverage in the TiO_2 photoanode when LA is used as a co-adsorbent, leading to enhanced J_{SC} [8, 9, 27]. Integrated current density (mA cm^{-2}) obtained from the IPCE curve of the DSSCs with

Table 6 The photovoltaic parameters and materials used in other DSSCs based on co-adsorbent modified photoanodes

Materials used	Co-adsorbent	Photovoltaic parameters		Efficiency (η) %	References
		V_{OC} (mV)	J_{SC} (mA cm^{-2})		
N719 dye Liquid electrolyte	Phenylalkonic acid	740	14.11	7.25	[20]
Z-907 Na Liquid electrolyte	Pivalic acid	735	11.80	6.25	[23]
N719 dye Liquid electrolyte	Oleic acid	786	15.39	7.65	[9]
D149 indoline dye Liquid electrolyte	Butyric acid	580	10.10	4.22	[8]
	Octanoic acid	580	10.20	4.18	
	Lauric acid	570	8.60	3.61	
	Stearic acid	580	5.30	1.97	
	Cholic acid	610	8.80	3.89	
N719 and RhCL dyes Liquid electrolyte	Formic acid (FA)	705	8.43	3.78	[7]
	Oxalic acid (OA)	719	9.13	4.59	
	Citric acid (CA)	673	8.24	3.75	
N719 dye Liquid electrolyte	1-Naphthalenetic acid (NAA) acid	619	14.47	5.91	[24]
N719 dye Liquid electrolyte	Poly(4-vinylbenzoic acid)	730	15.7	8.3	[25]
	Poly(4-vinylpyridine)	730	17.4	9.0	
N719 dye Liquid electrolyte	LA	662	20.54	8.31	This work

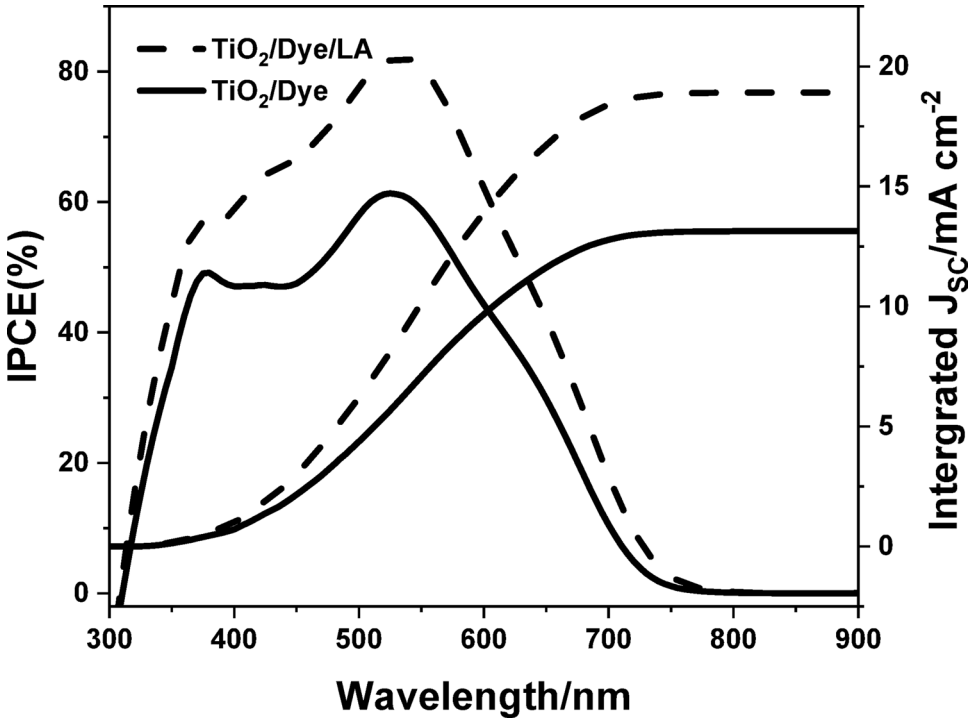

Fig. 6 The IPCE curves of the DSSCs with pristine TiO_2/Dye photoanode and LA anchored TiO_2/Dye photoanode

Table 7 Integrated current density (mA cm^{-2}) of the DSSCs with pristine TiO_2/Dye photoanode and LA anchored TiO_2/Dye photoanode

Photo anode	Integrated current density (mA cm^{-2})	Current density from I–V measurements (mA cm^{-2})
TiO_2/Dye	13.2	14.9
TiO_2/Dye/LA	18.9	20.5

pristine TiO_2/Dye photoanode and LA anchored TiO_2/Dye photoanode are given in the Table 7.

According to Khazraji et al. the IPCE of a merocyanine dye-sensitized TiO_2 solar cell has improved with the addition of a co-adsorbent, preventing the formation of a dimer, which has lower electron-injection performance compared to the monomer [31]. Xiaoming Ren et al. reported that DCA or DCNa used as co-adsorbents act as spacers among dye molecules, thus suppressing the π-π interaction of the dye molecules, which inhibits charge recombination and hence improves the IPCE significantly [57].

According to the IPCE spectra reported by Mazloum et al. [9] on the Oleic Acid (OA) incorporated system, the enhanced quantum field is attributed to oleic acid as a co-adsorbent, which reduces dye aggregation, minimizes energy loss, and improves electron injection efficiency. In comparison, in the present study, the increasing current density due to the incorporation of LA as a co-adsorbent can be interpreted based on a similar mechanism. The observed IPCE improvements in our experiments are also consistent with the literature [8].

3.5 Mott–Schottky analysis

The Mott–Schottky (or M-S) plots involve measuring capacitance against electrode potential under depletion conditions. According to M-S theory, a straight line in the dC_{SC}/dE plot with constant intercept at the flat band potential (E_f) is independent of time and polarization. Figure 7 shows the M-S plots for both pristine TiO_2/Dye and LA-anchored TiO_2/Dye devices. The measurements were conducted under dark conditions, and the applied potential was varied between −1.0 and + 1.0 V to examine the shift in E_f of TiO_2 caused by LA molecule adsorption on TiO_2 surface [58].

In the DSSC, the open circuit voltage (V_{OC}) coincides with the energy difference ΔE between the Fermi levels of TiO_2 E_f and the reduction potential of the redox electrolyte E_{redox} [59]. The value of V_{OC} is given by the Eq. 3 (Supplementary Information).

According to equation S3, it is clear that the change of flat band potential must be one of the reasons for the change in the value of (V_{OC}). In this case, the E_f of the pristine TiO_2 and LA-LA-anchored TiO_2 are approximately −0.269 V and −0.210 V, respectively. This suggests that upon LA modification, the E_f of TiO_2 is shifted toward a positive direction concerning the redox potential of the electrolyte (E_{redox}), resulting in a decrease in (V_{OC}).

The surface modification of TiO_2 with an acid resulted in a positive shift of the quasi-Fermi level, while the treatment with a base resulted in the shift of the E_f toward negative potential. According to photovoltaic performance, the LA anchored TiO_2/Dye photoanode showed a lower V_{OC} of 669

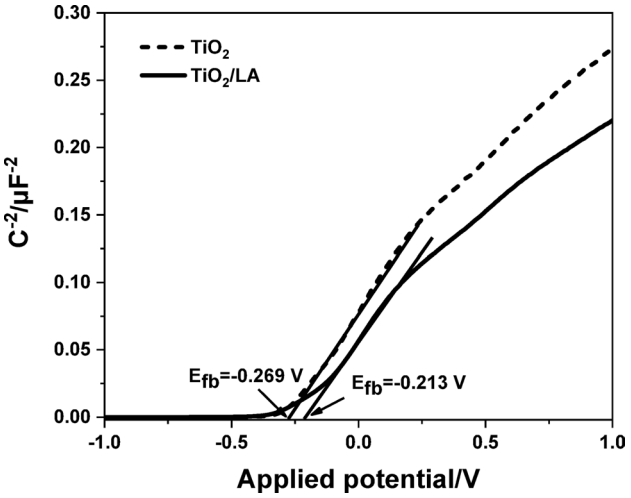

Fig. 7 Mott–Schottky plots measured at a frequency of 1 kHz of the DSSCs with pristine TiO_2/Dye photoanode and LA anchored TiO_2/Dye photoanode under dark conditions

mV, while that of the pristine TiO_2/Dye photoanode showed a V_{OC} of 723 mV. Therefore, as illustrated in Fig. 8, there is a decrease in V_{OC} by approximately 60 mV. In Fig. 8, E_{VB} is the valence band maximum;E_{CB} is the conduction band maximum; E_f is the Quasi-fermi energy; E_{redox} is the Red-ox potential of the electrolyte; V_{OC1} is the open circuit voltage on TiO_2/Dye photoanode; V_{OC2} is the open circuit voltage on TiO_2/Dye/LA photoanode.

However, this shift toward a positive direction is favorable for the efficient charge injection from the dye molecule to the conduction band of the TiO_2, contributing to the higher cell efficiency for the DSSC with LA anchored TiO_2. In addition, the built-in potential, which is the difference between the E_f value of LA-modified and pristine TiO_2 photoanodes, was determined to be 60 mV upon LA modification of TiO_2 device. This potential difference serves as the main driving force for the enhanced charge separation and reduced back electron transfer from TiO_2 to I_3^- [22, 58]. The positive shift in E_f is expected to raise the work function of the TiO_2 photoanode, given that the work function represents the energy needed to move an electron from E_f to vacuum. This difference can be partially attributed to the electron-withdrawing nature of the –COOH group of LA moiety that directs the dipole away from the TiO_2 surface [5]. Theoretically, the charge carrier density of a semiconductor material is inversely proportional to the slope of the Mott-Schottky. Therefore, the decrease in the slope in the linear portion of the Mott–Schottky curve of LA anchored TiO_2/Dye photoanode corresponds to the higher carrier concentration [60]. The charge carrier type of the semiconductor can also be deduced from the slope of the M-S plots: a positive slope like seen in Fig. 7, signifies n-type carrier conduction [61].

Moreover, As observed in the FTIR studies, linoleic acid (LA) gets bonded with TiO_2 via −COOH groups, similar to the protonation effect observed with ruthenium dyes like N3 and N719. Linoleic acid may donate protons to the TiO_2 surface, resulting in a positive surface charge and a downward shift of the Fermi level. This shift can reduce the V_{OC}. However, the hydrophobic tail of LA may also help suppress charge recombination, partially compensating for the V_{OC} loss and contributing to improved device stability [62].

The change in VOC can be further described using Cyclic Voltammetry and Electrochemical Impedance Spectroscopy (EIS) Analyses in the following sections.

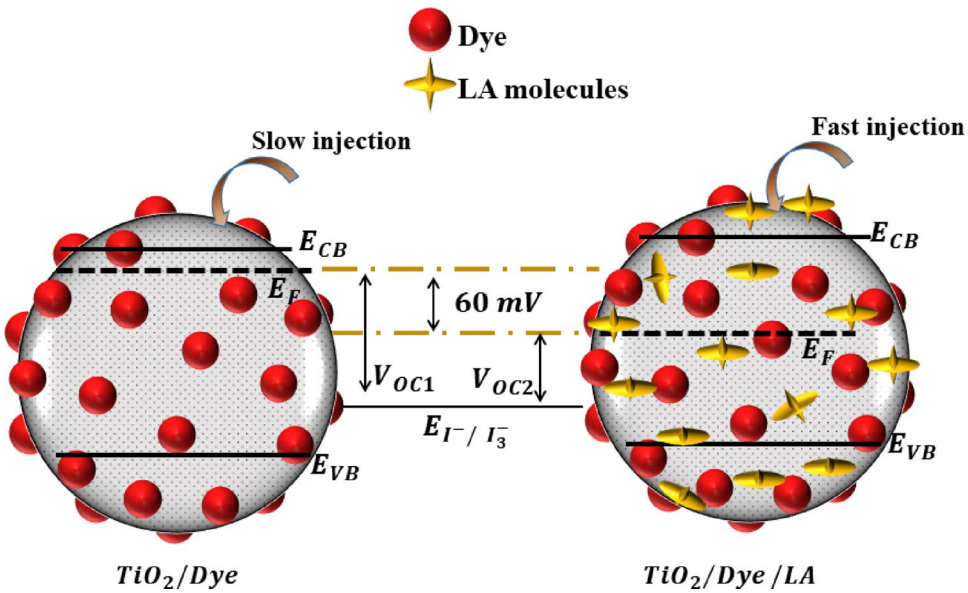

Fig. 8 The effect of LA modification in tuning the E_f of TiO_2; TiO_2/Dye and TiO_2/Dye/LA photoanodes with the E_f shifting toward the red-ox potential of the I_3^-/I^-

3.6 Cyclic voltammetry analysis

According to Eq. 4 (supplementary information), the position of the Fermi level (E_f) is influenced by both the position of E_{CB} and the number of electrons in TiO_2 (*n)*. To further confirm this, Cyclic voltammetry measurements were performed on a pristine TiO_2/Dye photoanode and LA anchored TiO_2/Dye photoanode. These measurements aimed to examine changes in trap states induced by LA, identify shifts in conduction band energy, and changes in V_{OC}. Figure 9(a) shows cyclic voltammograms of pristine TiO_2/Dye photoanode and LA-anchored TiO_2/Dye photoanode in the electrolyte solution.

Basically, cyclic voltammograms can be used to determine the energy distribution of acceptor states at the TiO_2 electrode surface since the current I (V) is proportional to the differential capacity (C) in a linear sweep. Therefore, the total injected charge (Q) can be calculated by integration by Eq. 5 (supplementary information).

The final energy level diagram is shown in Fig. 9(b) as a function of the electrode potential [63, 64].

For the above CV measurements, platinum was used as the counter electrode, Ag/AgCl as the reference electrode,

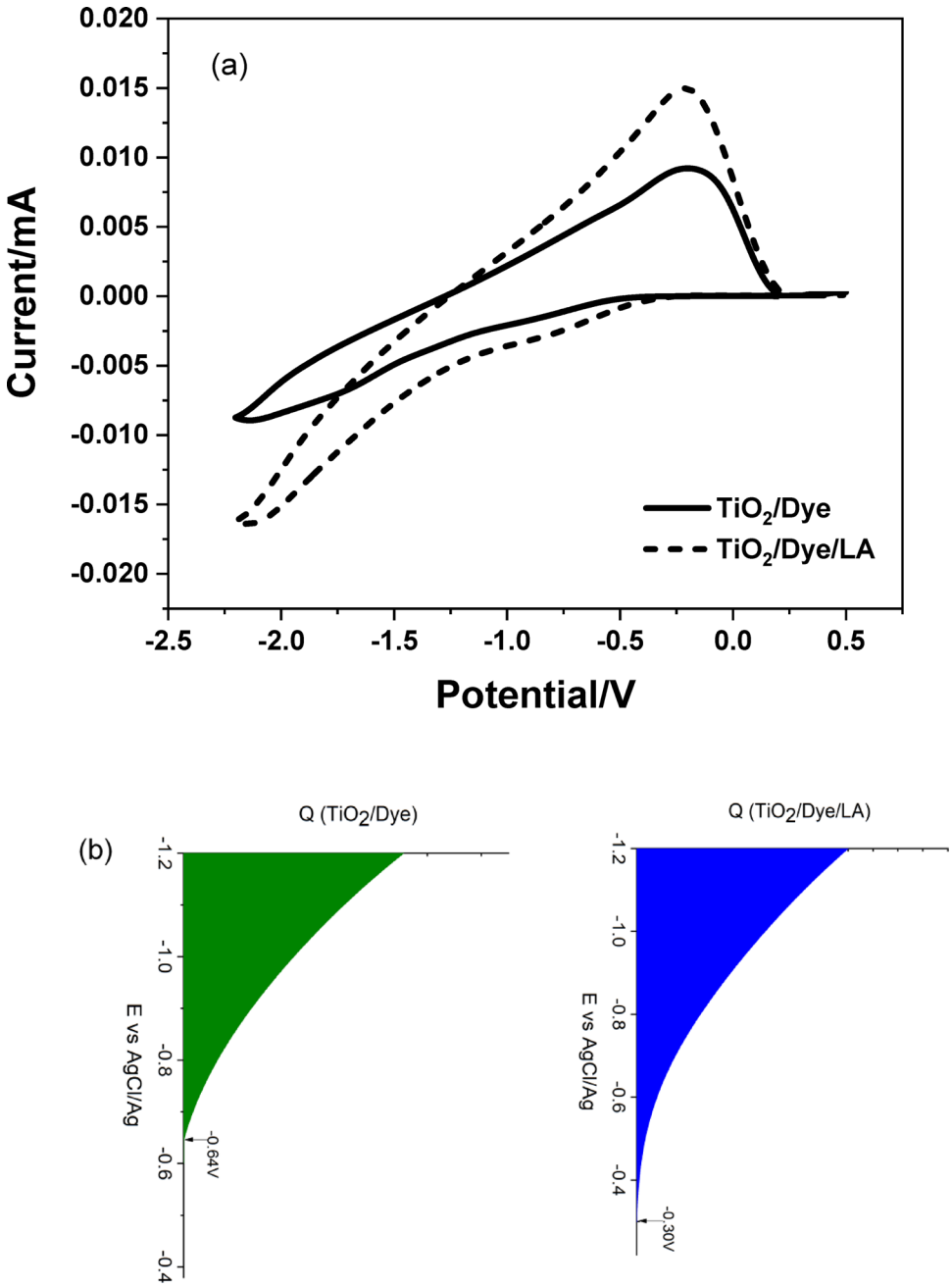

Fig. 9 **a** Cyclic voltammograms of pristine TiO_2/Dye photoanode and LA anchored TiO_2/Dye photoanode in electrolyte solution and **b** energy levels at the TiO_2/electrolyte interface

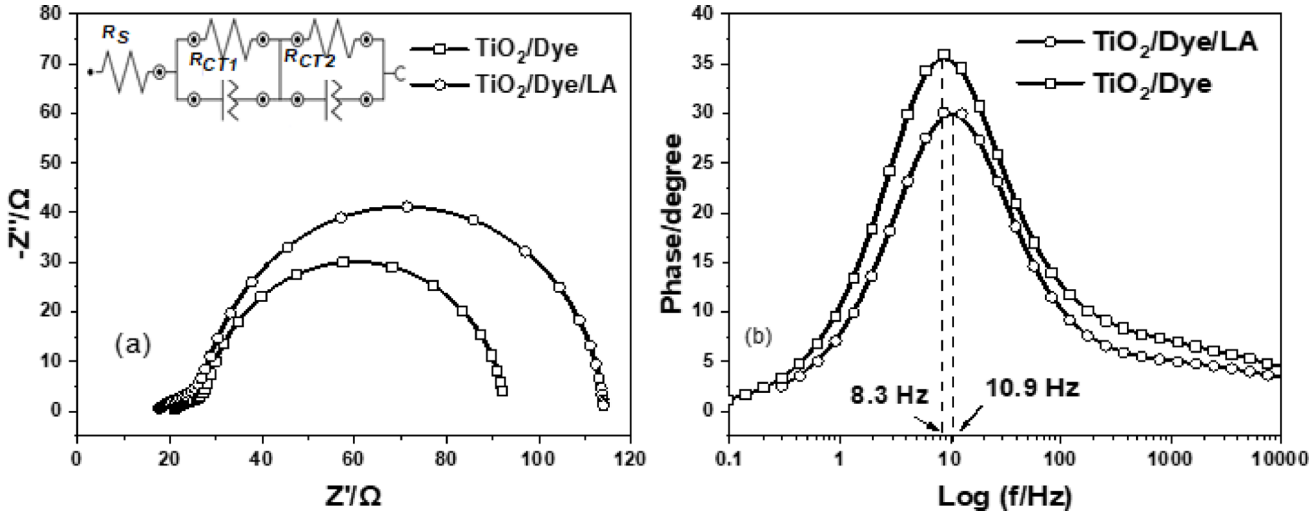

Fig. 10 **a** EIS Nyquist plots of DSSCs made with two TiO_2 photoanodes, with and without LA, and **b** the Bode plots corresponding to the EIS spectra of (**a**)

Table 8 Electron transport parameters of DSSCs extracted from EIS analysis

Photoanode	R_S (Ω)	R_{CT1} (Ω)	R_{CT2} (Ω)	τ (ms)	C_μ (μF)	D_{eff} ($m^2\ s^{-1} \times 10^{-9}$)	L_{eff} (μm)	η_{cc} ($m^{-3} \times 10^{22}$)	τ_d (ms)
TiO_2/Dye	20.30 ± 0.47	9.03 ± 1.17	63.6 ± 1.79	19.17	174.7	5.58	10.2	2.79	3.54
TiO_2/Dye/LA	16.9 ± 0.41	13.7 ± 2.13	83.6 ± 2.58	14.60	301.5	6.01	11.8	4.82	5.09

while maintaining a scan rate 50 mV/s. The capacitive currents during the forward scan of the electrodes showed gradual onsets. For instance, the onset potential was approximately − 0.64 V for the pristine TiO_2/Dye electrode in direct contact with the electrolyte, whereas the LA anchored TiO_2/Dye photoanode exhibited an onset at − 0.37 V. This observation suggests a slight change that allows current to be produced at lower potentials in the conduction band edge of TiO_2, subsequently lowering V_{OC} values [9, 65, 66]. Alagar Ramar et al. also confirmed from their studies that the incorporation of poly(N-vinylcarbazole) (PVK) in the TiO_2 photoanode facilitates proton transfer, leading to a gradual downward shift in the Fermi level of electrons in TiO_2 and subsequently lowering the V_{OC} values. Cyclic voltammetry data confirmed these changes, showing an anodic shift in onset potentials with increased PVK loading, indicating a positive shift in the TiO_2 conduction band [67].

3.7 Electrochemical impedance spectroscopy (EIS) analysis

The utilization of electrochemical impedance spectroscopy (EIS) is well recognized as a highly effective technique for acquiring insights into the electron-transport mechanisms within DSSCs [68]. EIS measurements were taken on each TiO_2 electrode sensitized with Dye alone and with Dye and LA to examine the effect of LA on the electron transport in TiO_2. Impedance data obtained were analyzed using equivalent electrical circuit models and NOVA software, allowing estimation of EIS parameters. The best fitting was obtained for the equivalent circuit shown in the inset and the resistance values were extracted from the best fit.

The Nyquist plots shown in Fig. 10a are made up of two semicircles. The resistance at the TiO_2/electrolyte interface is responsible for the larger semicircle at lower frequencies, while the smaller one at higher frequencies indicates the charge-transfer resistance at the counter electrode/electrolyte interface. Table 8 lists the electron transport parameters that have been extracted from the equivalent circuit shown in the inset of Fig. 10a. The total series resistance (R_S), charge-transfer resistance at the Pt/electrolyte interface (R_{CT1}), and recombination resistance at the TiO_2/dye/electrolyte interface (R_{CT2}) were determined using NOVA software and are represented in the equivalent circuit [9, 21, 69].

The total series resistance R_S was slightly reduced from 20.3 to 16.9 Ω. The charge-transfer resistance at the Pt/electrolyte interface of LA-treated TiO_2 photoanode R_{CT1} was slightly changed from 9.03 to 13.7 Ω. LA-anchored TiO_2/Dye photoanode showed a higher charge recombination resistance R_{CT2} (83.6 Ω) compared to the unmodified device (63.6 Ω), indicating that the back electron transport was reduced upon LA modification. This confirms that DSSCs with LA-anchored TiO_2/Dye photoanode experience reduced recombination rates at the photoanode/electrolyte interface [5].

It can be suggested that high recombination resistance might be responsible for a higher V_{OC}. However,

Mott–Schottky analysis strongly indicated a decrease in V_{OC} for the modified device. This observation is further supported and aligned with the notable increase in J_{OC} of LA anchored TiO_2/Dye photoanode. Thus, LA molecules can effectively boost the charge transfer rate due to the COO– groups present in LA. This enhancement in charge transfer contributes to the enhancement of J_{OC} and ultimately improves the efficiency of these devices.

As illustrated in Fig. 10b, the Bode phase plots display the frequency peaks associated with the charge transfer processes for TiO_2 electrodes sensitized with dye alone and with LA. The electron lifetime (τ) was calculated using Eq. 6 (supplementary information),

The maximum frequencies ($f_{\max}$) observed are 8.3 Hz for the TiO_2 electrode sensitized with the dye alone and 10.9 Hz for those incorporated with dye and LA. Corresponding to these results, the calculated electron Lifetime has changed from 19.17 to 14.60 ms, due to the incorporation of LA to the photoanode. Calculated electron lifetime values are tabulated in Table 8. From these values, it is evident that the effective electron life time is shorter in the DSSCs with the LA.

Moreover, further electrochemical parameters were extracted for both the modified and unmodified devices. The chemical capacitance C_μ was calculated using Eq. 7 (supplementary information), the increased C_μ observed in the modified device shows an enhanced electron density in the TiO_2 semiconductor. Effective electron diffusion coefficient (D_{eff}), which represents the concentration of electrons that diffuse into the photanode, was calculated by using Eq. 8 (supplementary information) A higher value of D_{eff} essential for improving the efficiency of a solar cell. The effective diffusion length was calculated using Eq. 9 (supplementary information). And should be greater than the thickness of the TiO_2 film (12 µm). In our case, however, both devices show nearly the same values as the thickness of the TiO_2 film. This may indicate that they are likely to undergo recombination before they can be fully injected into the conduction band and diffuse across the TiO_2 film. LA anchored photoanode (5.09 ms) exhibited higher electron transport time (τ_d) (Eq. 11, supplementary information) than the unmodified device (3.54 ms). The electron density (η_s), which is calculated using Eq. 10 (Supplementary Information) of the modified photoanode (4.82×10^{22} m^{-3}) higher than that of the unmodified device 2.79×10^{22} m^{-3}, thereby enhancing the number of electrons available for transport through the external circuit without significant recombination, as the higher electron density per unit volume facilitates more efficient charge collection [70–74].

Since the impedance measurements were conducted under light conditions, shorter life time at the photoanode lead to faster charge transfer, easy charge diffusion, and reduced recombination. Therefore, LA on the TiO_2 surface has promoted the charge transfer and increased the rate of electrons reaching the collecting electrode. This shorter electron life time in the modified photoanode is evident in the enhancement of J_{SC}, reduction of $V_{OC,}$ as well as in the overall efficiency of the solar cell [75, 76].

4 Conclusion

Based on this study, LA is proposed as a novel co-adsorbent for TiO_2 photoanode in DSSCs due to its ability to hinder recombination processes at the photoanode/electrolyte interface without impeding charge injection from the dye to TiO_2, thus enhancing the efficiency in DSSCs through surface engineering of TiO_2 of the photoanode/electrolyte interface. The optimized TiO_2/Dye/LA photoanode-based device (0.95 mM) achieved an efficiency of 8.31% under the illumination of 100 mW cm^{-2} (AM 1.5), a significant improvement over the unmodified TiO_2/Dye photoanode-based device with an efficiency of 6.61%. This photoanode modification resulted an impressive 38% increase in J_{SC} values and an overall efficiency enhancement of 25%. The interaction between iodine and the double bonds of LA appears to play a crucial role in reducing recombination rates by limiting iodine binding to dye molecules. This interaction increases the distance between TiO_2 and acceptors in the electrolyte, fostering efficient charge injection from dye molecules to the conduction band of TiO_2, thereby contributing to the higher efficiency observed in the DSSC with LA anchored TiO_2 photoanode. Additionally, the removal of excess aggregated dye molecules by LA molecules and the creation of surface electronic states by LA anchoring on the TiO_2 surface further facilitate charge transfer without impeding charge injection. This work emphasizes the potential of organic interface engineering approaches for achieving high-efficiency, low-cost solar energy conversion.

Supplementary Information The online version contains supplementary material available at https://doi.org/10.1007/s10800-025-02352-8.

Author contributions MAKLD: Conceptualization, supervision, checking data, editing manuscript. PUS: Investigation, data curation, methodology, formal analysis, writing—original draft. GKRS: Conceptualization, supervision, checking data, editing manuscript. JMKWK: Supervision, checking data, editing manuscript. MSHH, JLS, AKK, WIS: Methodology, curation of data, preparation of figures and tables.

Funding Most laboratory facilities, Research Assistance and main resources (Chemicals and equipment) were provided by National Institute of Fundamental Studies, Kandy, Sri Lanka.

Data availability No datasets were generated or analysed during the

current study.

Declarations

Conflict of interest The authors declare that they have no known competing financial interests or personal relationships that could have appeared to influence the work reported in this paper.

References

1. Tutar ÖF, Öztürk N, Bekmez MG et al (2024) Enhanced performance of dye-sensitized solar cells via anthocyanin, chlorophyll, benzothiadiazole and diphenylacridine co-sensitizers and amine-based co-adsorbents. Opt Mater (Amst). https://doi.org/10.1016/j.optmat.2024.116207
2. Ebrahim K (2011) Dye sensitized solar cells—working principles, challenges and opportunities. Sol Cells Dye Devices. https://doi.org/10.5772/19749
3. Subhan A, Dharmalingam K, Mourad AHI et al (2025) Improved photovoltaic performance of dye-sensitized solar cell upon doping with pulsed-laser fabricated plasmonic silver nanoparticles as modified photoanodes. Mater Renew Sustain Energy. https://doi.org/10.1007/s40243-025-00315-9
4. O'Regan B, Grätzel M (1991) A low-cost, high-efficiency solar cell based on dye-sensitized colloidal TiO2 films. Nature 353:737–740
5. Gopalraman A, Karuppuchamy S, Vijayaraghavan S (2019) High efficiency dye-sensitized solar cells with: VOC-JSC trade off eradication by interfacial engineering of the photoanode|electrolyte interface. RSC Adv 9:40292–40300. https://doi.org/10.1039/c9ra08278f
6. Mendive CB, Blesa MA, Bahnemann D (2007) The adsorption and photodegradation of oxalic acid at the TiO_2 surface. Water Sci Technol 55:139–145. https://doi.org/10.2166/wst.2007.398
7. Saxena V, Veerender P, Gusain A et al (2013) Co-sensitization of N719 and RhCL dyes on carboxylic acid treated TiO_2 for enhancement of light harvesting and reduced recombination. Org Electron 14:3098–3108. https://doi.org/10.1016/j.orgel.2013.07.020
8. Magne C, Urien M, Ciofini I et al (2012) Amphiphilic acids as co-adsorbents of metal-free organic dyes for the efficient sensitization of nanostructured photoelectrode. RSC Adv 2:11836–11842. https://doi.org/10.1039/c2ra22121g
9. Mazloum-Ardakani M, Khoshroo A (2015) Enhanced performance of dye-sensitized solar cells with dual-function coadsorbent: reducing the surface concentration of dye-iodine complexes concomitant with attenuated charge recombination. Phys Chem Chem Phys 17:22985–22990. https://doi.org/10.1039/c5cp03428k
10. Gong J, Sumathy K, Qiao Q, Zhou Z (2017) Review on dye-sensitized solar cells (DSSCs): advanced techniques and research trends. Renew Sustain Energy Rev 68:234–246. https://doi.org/10.1016/j.rser.2016.09.097
11. Karim NA, Mehmood U, Zahid HF, Asif T (2019) Nanostructured photoanode and counter electrode materials for efficient dye-sensitized solar cells (DSSCs). Sol Energy 185:165–188. https://doi.org/10.1016/j.solener.2019.04.057
12. Zhou H, Aftabuzzaman M, Masud N et al (2025) Key materials and fabrication strategies for high-performance dye-sensitized solar cells: comprehensive comparison and perspective. ACS Energy Lett 10:881–895. https://doi.org/10.1021/acsenergylett.4c03579
13. Chappidi VR, Seshaiah KV, Madduri S, Raavi SSK (2024) Rare-earth-doped TiO2 photoanode DSSCs for indoor photovoltaics: a comparative study. J Mater Sci Mater Electron 35:1–13. https://doi.org/10.1007/s10854-024-12261-9
14. Hore S, Kern R (2005) Implication of device functioning due to back reaction of electrons via the conducting glass substrate in dye sensitized solar cells. Appl Phys Lett 87:1–3. https://doi.org/10.1063/1.2149215
15. Hao S, Wu J, Fan L et al (2004) The influence of acid treatment of TiO2 porous film electrode on photoelectric performance of dye-sensitized solar cell. Sol Energy 76:745–750. https://doi.org/10.1016/j.solener.2003.12.010
16. Kay A, Grätzel M (1993) Artificial photosynthesis. 1. Photosensitization of TiO_2 solar cells with chlorophyll derivatives and related natural porphyrins. J Phys Chem 97:6272–6277. https://doi.org/10.1021/j100125a029
17. Kusama H, Arakawa H (2004) Influence of benzimidazole additives in electrolytic solution on dye-sensitized solar cell performance. J Photochem Photobiol Chem 162:441–448. https://doi.org/10.1016/S1010-6030(03)00414-3
18. Das P, Sengupta D, Kasinadhuni U et al (2015) Nano-crystalline thin and nano-particulate Thick TiO_2 layer: cost effective sequential deposition and study on dye sensitized solar cell characteristics. Mater Res Bull 66:32–38. https://doi.org/10.1016/j.materresbull.2015.02.018
19. Fei C, Tian J, Wang Y et al (2014) Improved charge generation and collection in dye-sensitized solar cells with modified photoanode surface. Nano Energy 10:353–362. https://doi.org/10.1016/j.nanoen.2014.10.007
20. Nath NCD, Lee HJ, Choi WY, Lee JJ (2013) Effects of phenylalkanoic acids as co-adsorbents on the performance of dye-sensitized solar cells. J Nanosci Nanotechnol 13:7880–7885. https://doi.org/10.1166/jnn.2013.8117
21. Wang P, Zakeeruddin SM, Humphry-Baker R et al (2003) Molecular-scale interface engineering of TiO_2 nanocrystals: improving the efficiency and stability of dye-sensitized solar cells. Adv Mater 15:2101–2104. https://doi.org/10.1002/adma.200306084
22. Anantharaj G, Lakshminarasimhan N (2018) Interfacial modification of photoanode|electrolyte interface using oleic acid enhancing the efficiency of dye-sensitized solar cells. ACS Omega 3:18285–18294. https://doi.org/10.1021/acsomega.8b02648
23. Li X, Lin H, Zakeeruddin SM et al (2009) Interface modification of dye-sensitized solar cells with pivalic acid to enhance the open-circuit voltage. Chem Lett 38:322–323. https://doi.org/10.1246/cl.2009.322
24. Şahingöz R, İldeş C, Çavuş HK (2024) Improving effects of 1-naphthalenetic acid (NAA) as a co-adsorbent on photovoltaic parameters of dye-sensitized solar cells. J Opt. https://doi.org/10.1007/s12596-024-01886-y
25. Rodrigues DFSL, Martins J, SAUVAGE F et al (2024) Suppression of back electron recombination on the photoanode-electrolyte interface with poly(4-vinylbenzoic acid) and poly(4-vinylpyridine) co-adsorbents for stable and efficient dye-sensitized solar cells. Surf Interfaces. https://doi.org/10.1016/j.surfin.2023.103627
26. Castillo-Robles JA, Rocha-Rangel E, Ramírez-De-león JA et al (2021) Advances on dye-sensitized solar cells (DSSCs) nanostructures and natural colorants: a review. J Compos Sci 5:1–25. https://doi.org/10.3390/jcs5110288
27. Jeong H, Chitumalla RK, Kim DW et al (2019) The comparative study of new carboxylated 1,3-indanedione sensitizers with standard cyanoacetic acid dyes using co-adsorbents in dye-sensitized solar cells. Chem Phys Lett 715:84–90. https://doi.org/10.1016/j.cplett.2018.11.026
28. Sayama K, Tsukagoshi S, Hara K et al (2002) Photoelectrochemical properties of J aggregates of benzothiazole Merocyanine dyes

on a nanostructured TiO_2 film. J Phys Chem B 106:1363–1371. https://doi.org/10.1021/jp0129380
29. Cole LZ and JM (2017) Dye aggregation in dye-sensitized solar cells. J Mater Chem 37:19541–19559
30. Adachi M, Sakamoto M, Jiu J et al (2006) Determination of parameters of electron transport in dye-sensitized solar cells using electrochemical impedance spectroscopy. J Phys Chem B 110:13872–13880. https://doi.org/10.1021/jp061693u
31. Khazraji AC, Hotchandani S, Das S, Kamat PV (1999) Controlling dye (Merocyanine-540) aggregation on nanostructured TiO_2 films. An organized assembly approach for enhancing the efficiency of photosensitization. J Phys Chem B 103:4693–4700. https://doi.org/10.1021/jp9903110
32. Muller JG, Karthikeyan J, Murugan P, Lakshminarasimhan N (2014) Influence of structural polymorphs on tunable white light generation from orange-red-emitting BiPO4:Eu3+ phosphor by surface modification. J Phys Chem C 118:19308–19314. https://doi.org/10.1021/jp505454n
33. Sekar S, Muller JG, Karthikeyan J et al (2018) Unveiling the multifunctional roles of hitherto known capping ligand oleic acid as blue emitter and sensitizer in tuning the emission colour to white in red-emitting phosphors. Phys Chem Chem Phys 20:19087–19097. https://doi.org/10.1039/c8cp02954g
34. Li L, Su Y, Li G (2010) Chemical modifications of red phosphor LaPO4: Eu3+ nanorods to generate white light. J Mater Chem 20:459–465. https://doi.org/10.1039/b917384f
35. Lu Y, Miller JD (2002) Carboxyl stretching vibrations of spontaneously adsorbed and LB-transferred calcium carboxylates as determined by FTIR internal reflection spectroscopy. J Colloid Interface Sci 256:41–52. https://doi.org/10.1006/jcis.2001.8112
36. López R, Gómez R (2012) Band-gap energy Estimation from diffuse reflectance measurements on sol-gel and commercial TiO_2: a comparative study. J Sol-Gel Sci Technol 61:1–7. https://doi.org/10.1007/s10971-011-2582-9
37. Scientific TF (2023) Band gap analysis through UV–visible spectroscopy. Thermo Fischer Inc
38. Lee DY, Park JH, Kim YH et al (2014) Effect of Nb doping on morphology, crystal structure, optical band gap energy of TiO_2 thin films. Curr Appl Phys 14:421–427. https://doi.org/10.1016/j.cap.2013.12.025
39. Lee DY, Kim JT, Park JH et al (2013) Effect of Er doping on optical band gap energy of TiO_2 thin films prepared by spin coating. Curr Appl Phys 13:1301–1305. https://doi.org/10.1016/j.cap.2013.03.025
40. Moloto W, Mbule P, Nxumalo E, Ntsendwana B (2024) Enhanced optical and electrochemical properties of FeBTC MOF modified TiO_2 photoanode for DSSCs application. Sci Rep 14:1–14. https://doi.org/10.1038/s41598-024-61701-3
41. Nakamura R, Tanaka T, Nakato Y (2004) Mechanism for visible light responses in anodic photocurrents at N-doped TiO_2 film electrodes. J Phys Chem B 108:10617–10620. https://doi.org/10.1021/jp048112q
42. Chen C, Xu L, Sewvandi GA et al (2014) Microwave-assisted topochemical conversion of layered titanate nanosheets to {010}-faceted anatase nanocrystals for high performance photocatalysts and dye-sensitized solar cells. Cryst Growth Des 14:5801–5811. https://doi.org/10.1021/cg501062r
43. Kharkwal D, Sharma N, Kumar Gupta S, Mohan Singh Negi C (2021) Enhanced performance of dye-sensitized solar cells by co-sensitization of metal-complex and organic dye. Sol Energy 230:1133–1140. https://doi.org/10.1016/j.solener.2021.11.037
44. Li X, Reynal A, Barnes P et al (2012) Measured binding coefficients for iodine and ruthenium dyes; implications for recombination in dye sensitised solar cells. Phys Chem Chem Phys 14:15421–15428. https://doi.org/10.1039/c2cp43347h
45. Luitel T, Zamborini FP (2013) Covalent modification of photoanodes for stable dye-sensitized solar cells. Langmuir 29:13582–13594. https://doi.org/10.1021/la402256v
46. Tsai MT (2002) Hydrolysis and condensation of forsterite precursor alkoxides: modification of the molecular gel structure by acetic acid. J Non Cryst Solids 298:116–130. https://doi.org/10.1016/S0022-3093(02)00918-3
47. Khan H, Swati IK, Younas M, Ullah A (2017) Chelated nitrogen-sulphur-codoped TiO_2: synthesis, characterization, mechanistic, and UV/Visible photocatalytic studies. Int J Photoenergy. https://doi.org/10.1155/2017/7268641
48. Vasconcelos DCL, Costa VC, Nunes EHM et al (2011) Infrared spectroscopy of Titania sol–gel coatings on 316L stainless steel. Mater Sci Appl 02:1375–1382. https://doi.org/10.4236/msa.2011.210186
49. Alsharaeh EH, Bora T, Soliman A et al (2017) Sol-gel-assisted microwave-derived synthesis of anatase Ag/TiO_2/Go nanohybrids toward efficient visible light phenol degradation. Catalysts. https://doi.org/10.3390/catal7050133
50. Rama Mohan T, Alice Branton T, Gopal Nayak DT (2015) Physical, spectroscopic and thermal characterization of biofield treated myristic acid. J Fundam Renew Energy Appl. https://doi.org/10.4172/2090-4541.1000180
51. Liascukiene I, Aissaoui N, Asadauskas SJ et al (2012) Ordered nanostructures on a hydroxylated aluminum surface through the self-assembly of fatty acids. Langmuir 28:5116–5124. https://doi.org/10.1021/la2051542
52. Premaratne WAPJ, Priyadarshana WMGI, Gunawardena SHP, De Alwis AAP (2014) Synthesis of Nanosilica from paddy husk Ash and their surface functionalization. J Sci Univ Kelaniya 8:33–48. https://doi.org/10.4038/josuk.v8i0.7238
53. Alcock BNW, Tracy VM, Sciences M (1976) 1976 Part 2. l Spectroscopic Studies. Group 1970–1973
54. Söderlind F, Pedersen H, Petoral RM et al (2005) Synthesis and characterisation of Gd2O3 nanocrystals functionalised by organic acids. J Colloid Interface Sci 288:140–148. https://doi.org/10.1016/j.jcis.2005.02.089
55. Liu Y, Scully SR, Mcgehee MD et al (2006) Dependence of band offset and open-circuit voltage on the interfacial interaction between TiO_2 and carboxylated polythiophenes. J Phys Chem 110(7):3257–3261
56. Barea EM, Zafer C, Gultekin B et al (2010) Quantification of the effects of recombination and injection in the performance of dye-sensitized solar cells based on N-substituted carbazole dyes. J Phys Chem C 114:19840–19848. https://doi.org/10.1021/jp1055842
57. Ren X, Feng Q, Zhou G et al (2010) Effect of cations in coadsorbate on charge recombination and conduction band edge movement in dye-sensitized solar cells. J Phys Chem C 114:7190–7195. https://doi.org/10.1021/jp911630z
58. Liu QP (2014) Analysis on dye-sensitized solar cells based on Fe-doped TiO2 by intensity-modulated photocurrent spectroscopy and Mott–Schottky. Chin Chem Lett 25:953–956. https://doi.org/10.1016/j.cclet.2014.03.025
59. Wali Q, Jose R (2019) SnO2 dye-sensitized solar cells. Nanomater Sol Cell Appl 205–285. https://doi.org/10.1016/B978-0-12-813337-8.00007-2
60. Bondarenko AS, Ragoisha GA (2005) Variable Mott–Schottky plots acquisition by potentiodynamic electrochemical impedance spectroscopy. J Solid State Electrochem 9:845–849. https://doi.org/10.1007/s10008-005-0025-7
61. Kunadian I, Lipka SM, Swartz CR et al (2009) Determination of carrier densities of boron- and nitrogen-doped multiwalled carbon nanotubes using Mott–Schottky plots. J Electrochem Soc 156:K110. https://doi.org/10.1149/1.3111032

62. Sharma K, Sharma V, Sharma SS (2018) Dye-sensitized solar cells: fundamentals and current status. Nanoscale Res Lett. https://doi.org/10.1186/s11671-018-2760-6
63. Zhang Z, Zakeeruddin SM, Regan BCO et al (2005) Influence of 4-guanidinobutyric acid as coadsorbent in reducing recombination in dye-sensitized solar cells. J Phys Chem 109(46):21818–21824
64. Wang Q, Zakeeruddin SM, Cremer J et al (2005) Cross surface ambipolar charge percolation in molecular triads on mesoscopic oxide films. J Am Chem Soc 127:5706–5713. https://doi.org/10.1021/ja0426701
65. Bakr ZH, Wali Q, Yang S et al (2018) Characteristics of ZnO-SnO2 composite nanofibers as a photoanode in dye-sensitized solar cells. Characteristics of ZnO-SnO_2 composite nanofibers as a photoanode in dye-sensitized solar cells. Ind Eng Chem Res 58(2):643–653. https://doi.org/10.1021/acs.iecr.8b03882
66. Vedavarshni S, Raguram T, Rajni KS (2020) Studies on the characteristics of TiO_2 photoanode and Flavanol pigment as a sensitiser for DSSC applications. Pramana. https://doi.org/10.1007/s12043-020-01982-1
67. Ramar A, Saraswathi R, Rajkumar M, Chen S (2015) Influence of Poly (N-vinylcarbazole) as a photoanode component in enhancing the performance of a dye sensitized solar cell influence of Poly (N-vinylcarbazole) as a photoanode component in enhancing the performance of a dye sensitized solar cell. J Phys Chem 119(42):23830–23838. https://doi.org/10.1021/acs.jpcc.5b06582
68. Adachi M, Noda K, Tanino R et al (2011) Comparison of electrochemical impedance spectroscopy between illumination and dark conditions. Chem Lett 40:890–892. https://doi.org/10.1246/cl.2011.890
69. Yavarzadeh M, Nasirpouri F, Foruzin LJ, Pourandarjani A (2024) Photocurrent response loss of dye sensitized solar cells owing to top surface Nanograss growth and bundling of anodic TiO_2 nanotubes. Heliyon 10:e24247. https://doi.org/10.1016/j.heliyon.2024.e24247
70. Du Z, Zhang H, Bao H, Zhong X (2014) Optimization of TiO_2 photoanode films for highly efficient quantum dot-sensitized solar cells. J Mater Chem A 2:13033–13040. https://doi.org/10.1039/c4ta02291b
71. Zhang J, Wang S, Ono K (2023) Electrochemical impedance spectroscopy. Microscopy and microanalysis for lithium-ion batteries. CRC, pp 301–350. https://doi.org/10.1201/9781003299295-11
72. Safie NE, Ludin NA, Hamid NH et al (2017) Electron transport studies of dye-sensitized solar cells based on natural sensitizer extracted from Rengas (*Gluta* spp.) and Mengkulang (*Heritiera elata*) wood. BioResources 12:9227–9243. https://doi.org/10.15376/biores.12.4.9227-9243
73. Srinivasa Rao S, Punnoose D, Venkata Tulasivarma C et al (2015) A strategy to enhance the efficiency of dye-sensitized solar cells by the highly efficient TiO_2/ZnS photoanode. Dalton Trans 44:2447–2455. https://doi.org/10.1039/c4dt03102d
74. Sharif M, Shafie NF, Ab S, Kadir MZA et al (2019) The effect of titanium (IV) chloride surface treatment to enhance charge transport and performance of dye-sensitized solar cell. Results Phys 15:1–7. https://doi.org/10.1016/j.rinp.2019.102725
75. Umair K, Dissanayake MAKL, Senadeera GKR (2021) Efficiency enhancement in SnO_2 based dye-sensitized solar cells by incorporating plasmonic gold nanoparticles. Ceylon J Sci 50:341. https://doi.org/10.4038/cjs.v50i5.7923
76. Marinado T, Nonomura K, Nissfolk J et al (2010) How the nature of triphenylamine-polyene dyes in dye-sensitized solar cells affects the open-circuit voltage and electron lifetimes. Langmuir 26:2592–2598. https://doi.org/10.1021/la902897z